Nanoscale

Accepted Manuscript

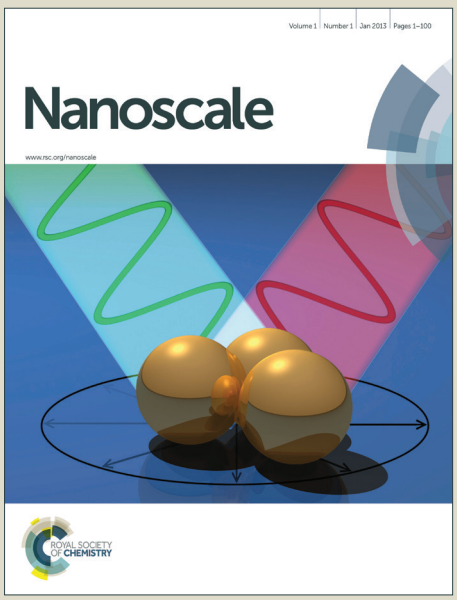

ROYAL SOCIETY OF CHEMISTRY

www.rsc.org/nanoscale

Controlled fabrication of porous double-walled TiO_2 nanotubes via ultraviolet-assisted anodization

Ghafar Ali, Hyun Jin Kim, Jae Joon Kim, and Sung Oh Cho*

Department of Nuclear and Quantum Engineering, Korea Advanced Institute of Science and Technology, Daejeon 305-701 (Korea), E-mail: socho@kaist.ac.kr

Abstract

Double-walled TiO_2 nanotubes with porous wall morphologies are fabricated by anodization under ultraviolet (UV) irradiation. TiO_2 forming by anodization of Ti is activated to generate electrons and holes by UV and the anodization process is influenced by the photo-generated charges. As a consequence, morphologies of the fabricated TiO_2 nanotubes can be adjusted by controlling the UV illumination. Double-walled TiO_2 nanotubes or single-walled nanotubes can be selectively formed by switching on/off the UV illumination. The thickness of the inner and outer walls of the double-walled nanotubes can be tailored by changing the UV power. Due to larger surface area compared to single-walled nanotubes, the porous double-walled nanotubes exhibit an enhanced photo-degradation rate for methylene blue. The mechanism of the porous double-walled TiO_2 nanotubes is proposed based on the photoactive semiconducting property of the as-growing TiO_2 nanotubes under UV.

Keywords: Anodization, UV irradiation, TiO_2 nanotubes, Double wall.

Introduction

Titanium dioxide (TiO_2) nanotubes have attracted great attention due to their promising application to solar cells [1], photocatalysis [2], water photo-splitting [3], drug delivery [4], bio-medical implants [5], sensors [6], and field emitters [7]. Among a few synthetic methods of TiO_2 nanotubes, electrochemical anodization is the most widely used because of its simplicity, versatility, low cost, and good controllability over morphology [8]. The performances of TiO_2 nanotubes in the applications greatly depend on both crystallinity and the surface areas of the nanotubes. The surface area of TiO_2 nanotubes can be increased by modifying the morphologies of the nanotubes. For example, nanotubes with porous [9], bamboo-like [10], branched [11] and double walls [12-15] have higher surface areas and accordingly exhibit better performances than nanotubes comprising compact and smooth walls [9, 14-16].

Meanwhile, it is well-known that crystalline TiO_2 has semiconducting properties and is activated to create electron-hole pairs by UV light due to its wide bandgap of 3.0 - 3.2 eV. TiO_2 nanotubes fabricated by anodization are generally amorphous, but amorphous TiO_2 is also a semiconductor of which bandgap (~3.4 eV) is slightly higher than that of crystalline TiO_2 [17, 18]. As a consequence, if UV is illuminated during anodization of Ti, electron-hole pairs can also be generated in the TiO_2 nanotubes forming by the anodization. These photo-generated electrons and holes can affect the anodization process, and thus, the morphologies or the properties of the TiO_2 nanostructures prepared by the UV-assisted anodization might be different from those fabricated by anodization without UV [19, 20].

Inspired by this possibility, we have tried systematic experiments on the anodization of Ti with and without UV irradiation. Here, we report that double-walled TiO_2 nanotubes with porous walls are fabricated by anodization of Ti under UV irradiation. The thickness of the inner and outer walls of the double-walled nanotubes can be tuned by changing the irradiated UV power. In addition, both single-

walled and double-walled TiO_2 nanotubes can be controllably synthesized by switching the UV light. The formation mechanism of the double-walled TiO_2 nanotubes is also discussed.

Experimental section

Prior to anodization, Ti sheets (0.1 mm thickness, 99.6% purity, Goodfellow, England) were cleaned by sonication in acetone, isopropyl alcohol, and methanol each for 10 min. Subsequently, the Ti sheets were rinsed with deionized water and dried in N_2 stream. The samples were anodized in a quartz cell containing ethylene glycol, EG (extra pure, Junsei, Japan) electrolyte, 0.5 wt.% NH_4F (Sigma-Aldrich), and 0.2 wt.% deionized water. The anodization process was carried out using a two-electrode system with a platinum sheet ($15 \times 25 \times 0.2$ mm^3) as a counter electrode and the Ti sheet as a working electrode. All the chemicals and materials were used in their as-received forms without any further purification. Anodization was conducted at a constant voltage of 60 V for 1h at room temperature using a DC power source. During the anodization, UV light was illuminated onto the Ti sheet using a 150 W Xe lamp. A low pass filter was used to cut off the light with the wavelength higher than 420 nm. The power density of the UV light reaching a Ti sheet was measured using a radiometer (ILT 1400-A, International Light Technologies, USA) and the power density was changed by inserting a plastic plate between the lamp and the quartz cell. Annealing of the nanotubes was carried out in air at 450 ˚C for 2h with a heating and a cooling rate of 3˚C /min.

The morphologies of the nanotubes were examined with a FESEM (Magellan 400, FEI Company, USA). The crystalline structures were characterized using a GAXRD (D/MAX 2500 V, Rigaku Corporation, Tokyo, Japan) using CuKα radiation (wavelength = 1.5406 Å). UV–vis diffuse reflectance spectra (DRS) of the single and doubled-wall TiO_2 nanotubes were obtained using a S-4100 spectrometer with a SA-13.1 diffuse reflector (Scinco Co. Ltd). Raman spectra were achieved using a high-resolution dispersive Raman spectrometer (Lab RAM HR, Horiba Jobin Yvon, France). A He–Ne laser producing 514 nm was used as the excitation source of the Raman spectrometer. XPS analysis was carried out under UHV conditions (10^{-10} Torr) with a spectrometer (Sigma Probe, Thermo VG

Scientific). The binding energies were calibrated using C1s peak (~ 284.8 eV) as the reference. The specific surface area and pore size distribution of the single and double-walled TiO_2 nanotubes attached on the Ti-substrate was measured by nitrogen (N_2) adsorption–desorption (ASAP 2420, Micromeritics) at 77.3 K and calculated by the Brunauer–Emmett–Teller (BET) method. The pore volume and the pore size distribution were derived using Barrett–Joyner–Halenda (BJH) model from the N_2 adsorption isotherm. The photocatalytic activities of the single and the double-walled TiO_2 nanotubes were determined by measuring the degradation rate of MB under UV-vis light generated by a 150 W Xe lamp. UV-vis light was illuminated into a quartz cell containing 2 mL of MB (100mg/L) aqueous solution and TiO_2 nanotubes. Prior to UV-vis illumination, the solution was put in a dark room for 30 min to ensure the adsorption-desorption equilibrium of the dye on the TiO_2 nanotubes. The relative concentration of MB in the solution was determined by comparing its UV-vis absorption intensity with that of the initial MB solution at the wavelength of 664 nm.

Results and discussion

Ti sheets were anodized under UV irradiation (see details in Experimental). Field-emission scanning electron microscope (FESEM) images of the as-anodized TiO_2 nanotubes prepared by the UV-assisted anodization are shown in Fig. 1. Top-view image of the nanotubes shows that double-walled TiO_2 nanotubes comprising inner walls and outer walls are formed (Fig. 1a). Bottom-view image (Fig. 1b) and the cross-sectional images (Fig. 1c, Fig. S1) of the nanotubes near the bottom also confirm the formation of double-walled nanotubes, and these furthermore indicate that the double-walled structures were created throughout their entire length of the nanotubes. The two walls are separated by ~10 nm from each other. Interestingly, the thickness of the inner and outer walls could be changed by changing the irradiated UV power. When the UV power density was 38 mW/cm^2, nanotubes with relatively thick (40 nm in average) inner walls and thin (20 nm in average) outer walls were obtained (Fig. 1a). However, when the UV power density was decreased to 20 mW/cm^2, the inner wall thickness was decreased to 20 nm while the outer wall thickness was increased to 40 nm, respectively (Fig. 1d). As a

result, nanotubes with relatively thin inner walls and thick outer walls were formed. The average pore diameters of the inner tubes and the outer tubes were 60 nm and 150 nm, respectively. For the comparison, when the anodization was carried out without UV illumination, only single-walled nanotubes were formed. Both FESEM image (Fig. 1e) and TEM image (Fig. S2) display that the nanotubes comprise only single walls and no interlayer is observed in the walls. The average pore diameter and the wall thickness of the single-walled nanotubes fabricated at the same anodization condition with that of the double-walled nanotubes were 125 nm and 25 nm, respectively. Therefore, single-walled or double-walled TiO_2 nanotubes can be controllably fabricated by anodization with or without UV irradiation (Fig. 1f). Moreover, the FESEM images of the front and the back sides of a Ti sheet further reveal the effect of the UV illumination on the morphologies of the TiO_2 nanotubes (Fig. S3). Only the front side of the Ti sheet was UV-irradiated during the anodization. Since both the front and the back sides were anodized simultaneously in the same electrolyte, other parameters such as temperature and pH value of the electrolyte are the same for both sides. Figure S3 shows that double-walled nanotubes were formed on the front side, but single-walled nanotubes were produced on the back side. This also demonstrates that UV irradiation is crucial for the formation of double-walled nanotubes. These facts can be used to fabricate unique and more complex TiO_2 nanotubes. For example, we did not illuminate UV light at an initial stage of the anodization and switched on a UV lamp after some time of the anodization. This leads to the formation of TiO_2 nanotubes comprising single walls at the upper parts and double walls at the bottom parts (Fig. 2). Single-walled nanotubes were initially fabricated without UV irradiation and then double-walled nanotubes were produced below the single-walled nanotubes by UV irradiation.

In addition, SEM images of the broken nanotubes (Fig. 1c; Fig. S1) clearly show that inner walls of the as-anodized double-walled nanotubes have porous structures while outer walls have compact and straight morphologies. When the as-prepared double-walled nanotubes were annealed at 450 ^{o}C for 2h, the inner walls became more porous and outer walls were also transformed into porous structures (Fig.

3). Both FESEM (Fig. 3a) and TEM images (Fig. 3b) clearly display the porous double-walled structures. XPS spectra show that C and F species as well as Ti and O are present in the as-anodized and annealed nanotubes (Fig. S4). C and F in the nanotubes are originated from the electrolyte [12, 21, 22]. However, the high resolution XPS spectra reveal that the content of C is drastically reduced in the double-walled nanotubes compared to the single-walled nanotubes (Fig. S5a), whereas F content is not changed (Fig. S5b). FTIR spectra (Fig. S6) also confirm this fact. Single-walled nanotubes show FTIR peaks at 1050 cm^{-1}, 1350 cm^{-1}, and 1450 cm^{-1}, which correspond to C-O stretching and C-H bending modes of the EG electrolyte [23]. These peaks demonstrate that carbonaceous species of the electrolyte are incorporated in the TiO_2 nanotubes [12, 21, 22]. However, intensities of these peaks are reduced in the as-anodized double-walled nanotubes (Fig. S6). Moreover, the UV-vis absorption spectrum (Fig. S7) of single-walled TiO_2 nanotubes shows higher absorption in the visible light region than that of doubled-wall nanotubes. These results indicate that the carbonaceous species are removed from the nanotubes by UV irradiation during the double-walled nanotube formation [24, 25]. In addition, annealing also affects the chemical composition of the double-walled nanotubes. Comparison of the XPS spectra shows that C and F contents are drastically reduced (Fig. S5a,b) and OH content is almost completely removed (Fig. S5c) after annealing of the double-walled nanotubes. All these results suggest that the removal of C, F, and OH species that are incorporated in the TiO_2 nanotubes affects the porous morphologies of the double-walled nanotubes. To be more exact, the removal of the carbonaceous species under UV mainly affects the inner wall morphology of the as-prepared double-walled nanotubes, and the removal of C, F and OH species by annealing makes both inner and outer walls more porous [12, 21, 22].

Annealing changed the crystalline structures as well as the morphologies of the nanotubes. The as-prepared double-walled nanotubes were amorphous as shown in the XRD spectra (Fig. 4a), but were transformed into anatase TiO_2 after the annealing. Raman spectra (Fig. 4b) further confirm the amorphous and anatase TiO_2 crystalline nature of the as-prepared and the annealed double-walled

nanotubes, respectively. Raman spectrum of the annealed nanotubes exhibits the vibrations at 146, 198, 399, 516, and 640 cm^{-1}, which correspond to the symmetries of E_g, B_{1g}, A_{1g}, and E_g modes of anatase TiO_2, respectively [26]. The crystalline structures of single-walled nanotubes were also transformed from amorphous to anatase by the annealing. However, the morphologies of the single-walled nanotubes were not changed so much after the annealing at the same condition with the double-walled nanotubes (Fig. S2).

The formation mechanism of the double-walled TiO_2 nanotubes is proposed as follows. If a Ti sheet is anodized in a fluoride-containing EG electrolyte, the fabricated nanotubes generally consist of TiO_2 (oxide) and $Ti(OH)_x$ (hydroxide) due to the reaction of Ti cations with O^{2-} and OH^- ions in the electrolyte [27]. Since OH^- ion is more bulky and has less charge than O^{2-} ion, the migration rate of OH^- across the metal/oxide interface is lower than that of O^{2-} [27, 28]. As a result, the nanotube's inner surface that contacts with the electrolyte includes more $Ti(OH)_x$ than TiO_2, while the nanotube's outer surface consists of more TiO_2 than $Ti(OH)_x$ [21, 22]. If UV is illuminated onto the TiO_2 nanotubes during anodization, electron-hole pairs are generated inside the nanotubes because the TiO_2 nanotubes have semiconducting properties even though they are amorphous structures [17 - 19]. In TiO_2 that has a n-type semiconducting property, holes tend to drift to nanotube/electrolyte interface due to the in-built potential [24, 29, 30]. More importantly, since an external potential is applied during the anodization process, holes easily migrate to the nanotube/electrolyte interface. The holes can convert a hydroxide bond to two hydroxide bonds through the interaction with a water molecule while releasing a H^+ ion to the electrolyte (Fig. S8) [24, 29, 30]. Moreover, it has been proposed that a small portion of trapped photogenerated holes can also transform titanium oxide into titanium oxy-hydoxide [24, 29, 30]. It has also been reported that the holes increase the migration of Ti^{4+} from metal-oxide interface towards oxide-electrolyte interface due to repulsive Coulomb forces [19]. As a results, more Ti^{4+} is ejected to the oxide-electrolyte interface (inner wall) where they react with water and form $Ti(OH)_x$ [21, 22]. Formation of such new hydroxide bonds was confirmed in our experiments. FTIR spectrum of the as-

prepared single-walled TiO_2 nanotubes exhibits broad band at 3000 ~ 3700 cm^{-1} (black line in Fig. S6), indicating the presence of Ti-OH bonds in the nanotubes [31]. However, the peak intensity of double-walled TiO_2 nanotubes prepared by UV irradiation increased (red line in Fig. S6), suggesting that more Ti-OH bonds were formed by UV [24, 29, 30]. Interestingly, we observed that when UV (power density of 38 mW/cm^2) was switched on during the anodization, the pH value of the electrolyte was rapidly decreased from 6.8 to 2.5 (Fig. S9). Decrease in the pH value during anodization indicates an relative increase in the concentration of H^+ in the electrolyte, which might be attributed to the decrease in the concentration of OH^- because OH^- is used to form Ti(OH) bond [24, 29]. XPS spectra (Fig. S5c) further demonstrate the formation of more Ti(OH) bonds by UV irradiation. An additional shoulder peak corresponding to Ti(OH) [32] can be seen in the as-prepared double-walled TiO_2 nanotubes besides the main oxygen peak. Hence, the inner surface of a nanotube gradually becomes a $Ti(OH)_x$-like material by UV irradiation [21, 22]. In addition, carbonaceous species originated from the electrolyte are incorporated into the nanotubes during the anodization, which is confirmed in our XPS (Fig. S5a) and FTIR (Fig. S6) results [12, 21, 22]. Therefore, a nanotube fabricated by UV-assisted anodization has two different layers in the wall: an inner layer that is mainly composed of Ti(OH) with carbonaceous species and an outer layer that mainly consists of TiO_2. However, the newly-formed singly coordinated Ti(OH) is not so stable and is converted to TiO_2 via dehydration [33] particularly under UV illumination [29, 30]. This results in a volume shrinkage of the inner layer, and hence, a gap is produced between the inner layer and the remained wall. Figure S1 displays that the inner surfaces of the outer walls have almost similar morphologies with the inner walls, suggesting that the two walls are originally connected with almost the same material. Moreover, UV irradiation removes carbonaceous species from the nanotube wall [24, 25], as already shown in (Fig. S5a). This accelerates the gap formation and simultaneously induces a porous inner wall [12]. Consequently, if a Ti is anodized under UV irradiation, double-walled TiO_2 nanotubes comprising porous inner walls and compact outer walls are created. Additionally, higher UV power produces more photogenerated holes and accordingly more Ti(OH)

formation at an inner layer, thereby resulting in double-walled nanotubes comprising thicker inner walls and thinner outer walls. The FESEM images, especially the two different cases of Fig. 1a and Fig. 1d, show that the outer walls of double-walled nanotubes are always thinner than the walls of single-walled nanotubes. This fact also supports our proposed mechanism for the formation of double-walled nanotubes.

Since the fabricated TiO_2 nanotubes have double walls with porous structures, the surface area of the nanotubes is much higher than that of the single-walled nanotubes [see the details in the Supporting Information], which is beneficial for photocatalytic applications. The photocatalytic activities of the single and double-walled anatase TiO_2 nanotubes were evaluated by photo-degradation of the methylene blue (MB) organic dye under UV□vis light generated by a Xe lamp. After 150 min of UV□vis light illumination, ~86 % of MB dye was decomposed by the single-walled TiO_2 nanotubes but almost 100 % of MB dye was decomposed by the double-walled TiO_2 nanotubes (Fig. 5). Hence the double-walled TiO_2 nanotubes exhibited better photocatalytic performance than the single-walled nanotubes.

Conclusions

In conclusion, we have presented a route to controllably fabricate double-walled TiO_2 nanotubes with porous walls by UV-assisted anodization. Double-walled or single-walled nanotubes can be prepared by switching on/off UV light, and the thickness of the inner and outer walls can also be tuned by changing the UV power. We propose that electron-hole pairs generated in the as-growing TiO_2 nanotubes by UV play an important role in the formation of the porous double-walled TiO_2 nanotubes. The porous double-walled nanotubes have larger surface areas than single-walled nanotubes and accordingly can exhibit better performances in various applications. Not only TiO_2 but also many other metal oxides formed by anodization also have photo-active semiconductor properties that are excited by UV. Therefore, the UV-assisted anodization technique can be expected to produce more interesting results, such as changes in the morphologies and the physical/chemical properties of various metal oxide

nanostructures.

Acknowledgements

This work was supported by the National Research Foundation of Korea (NRF) grant funded by the Korea government (MEST) (2013M2A8A1041415).

Supporting Information Available. FESEM images of double-walled TiO_2 nanotubes, TEM image of single-walled TiO_2 nanotubes, schematic drawing of single as well as double-walled TiO_2 nanotubes, XPS, FTIR, UV-vis absorption spectra, pH graph, N_2 adsorption-desorption isotherm, BET surface area, and pore size distribution of the single and doubled-wall TiO_2 nanotubes.

References

[1]. a) B. O. Regan and M. Gratzel, *Nature*, 1991, 353, 737. b) C. Chen, Y. Xie, G. Ali, S. H. Yoo and S. Oh Cho, *Nanotechnology*, 2011, 22, 015202. c) C. Chen, G. Ali, S. H. Yoo, J. M. Kum, S. Oh Cho, *J. Mater. Chem*., 2011, 21, 16430. d) C. Chen, Yi. Xie, G. Ali, S. H. Yoo and S. Oh Cho, *Nano. Res. Lett*., 2011, 6, 462.

[2]. Y. Xie, G. Ali, S. H. Yoo, and S. Oh Cho, *ACS App. Mater. Interf*., 2010, 2, 2910.

[3]. M. Altomare, K. Lee, M. S. Killian, E. Selli, and P. Schmuki, *Chem. Eur. J.* 2013, 19, 5841.

[4]. N. K. Shrestha, J. M. Macak, F. Schmidt-Stein, R. Hahn, C. T. Mierke, B. Fabry, P. Schmuki, *Angew. Chem. Int. Ed.,* 2009, 48, 969.

[5]. J. Park, S. Bauer, K. von der Mark and P. Schmuki, *Nano Lett.,* 2007, 7, 1686.

[6]. D. Spitzer, T. Cottineau, N. Piazzon, S. Josset, F. Schnell, S. N. Pronkin, E. R. Savinova, and V. Keller, *Angew. Chem. Int. Ed*., 2012, 51, 5334.

[7]. X. Xu, C. Tang, H. Zeng, T. Zhai, S. Zhang, H. Zhao, Y. Bando, and D. Golberg, *ACS App. Mater. Interf.,* 2011, 3, 1352.

[8]. a) S. Berger, R. Hahn, P. Roy, and P. Schmuki, *Phys. Status Solidi B,* 2010, 247, 2424. b) G. Ali, S. H. Yoo, J. M. Kum, Y. N. Kim and S. Oh Cho, *Nanotechnology,* 2011, 22, 245602. c) G. Ali, C. Chen, S. H. Yoo, J. M. Kum and S. Oh Cho, *Nano. Res. Lett*., 2011, 6, 332.

[9]. S. Wang, L. Liu, F. Zhang, K. Tao, E. Pippel, K. Domen, *Nano lett.* 2011, 11, 3649.

[10]. S. P. Albu, D. Kim, and P. Schmuki, *Angew. Chem. Int. Ed*., 2008, 47, 1916.

[11]. Z. Jin, G. T. Fei, X. Y. Hu, S. H. Xu, and L. De Zhang, *Chem. Lett.*, 2009, 38, 288.

[12]. a) S. P. Albu, A. Ghicov, S. Aldabergenova, P. Drechsel, D. Le Clere, G. E. Thompson, J. M. Macak, and P. Schmuki, *Adv. Mater.,* 2008, 20, 4135. b) S. P. Albu and P. Schmuki, *Phys. Stat. Solidi RRL*, 2010, 4, 215.

[13]. Y. Ji, K.-Chu Lin, H. Zheng, J.-jie Zhu, A. Cristina S. Samia, *Electro. Comm*., 2011, 13 1013.

[14]. S. E. John, S. K. Mohapatra, M. Misra, *Langmuir*, 2009, 25, 8240.

[15]. X. Zhang, F. Han, Bo. Shi, S. Farsinezhad, G. P. Dechaine, and K. Shankar, *Angew. Chem. Int. Ed.*, 2012, 51, 12732.

[16]. D. Kim, A. Ghicov, S. P. Albu and P. Schmuki, *J. Am. Chem. Soc.,* 2008, 130, 16455.

[17]. K. Eufinger, D. Poelman, H. Poelman, R. De Gryse, G. B. Marin, *App. Surf. Sci.,* 2007, 254, 148.

[18]. K. S. Raja, V. K. Mahajan, M. Misra, *J. Power. Sour.* 2006, 159, 1258.

[19]. Y. R. Smith, B. Sarma, S. K. Mohanty, M. Misra, *ACS App. Mater. & Interf., 2012,4, 5883.*

[20]. A. Hazra, S. K. Hazra, D. Dutta, C. K. Sarkar, S. Basu, *Frontiers in Sensors* 2013, 1, 17.

[21]. H. Mirabolghasemi, N. Liu, K. Lee and P. Schmuki, *Chem. Comm.*, 2013, 49, 2067.

[22]. N. Liu, H. Mirabolghasemi, K. Lee, S. P. Albu, A. Tighineanu, M. Altomare and P. Schumi, *Faraday Discussion*, 2013, 164, 107.

[23]. R. M. Silverstein, G. C. Bassler, T. C Morrill, Spectrometric identification of organic compounds, 4th Ed., New York, John Wiley and Sons, 1981.

[24]. K. Hashimoto, H. Irie and A. Fujishima, *Jap. J. App. Physics*, 2005, 44, 8269.

[25]. P. Roy, T. Dey, K. Lee, D. Kim, B. Fabry, and P. Schmuki, *J. Am. Chem. Soc.,* 2010, 132, 7893.

[26]. G. Ali, S. H. Yoo, J. M. Kum, H. S. Raza, D. Chen, S. Oh Cho, *J. Nanopart. Res.,* 2012 14, 1047.

[27]. B. Chen, J. Hou, K. Lu, *Langmuir*, 2013, 29, 5911.

[28]. Z. Su, W. Zhou, F. Jiang and M. Hong, *J. Mater. Chem.*, 2012, 22, 535.

[29]. A. Fujishima, X. Zhangb, D. A. Tryk, *Surf. Sci. Reports,* 2008, 63, 515.

[30]. N. Sakai, A. Fujishima, T. Watanabe, K. Hashimoto, *J. Phys. Chem. B.*, 2003, 107, 1028.

[31]. T. Lopez, R. Gomez, E. Sanchez, F. Tzompantzi and L. Vera, *J. Sol-Gel Sci. and Tech*., 2001, 22, 99.

[32]. H. J. Choi, M. Kang, *Intern. J. Hydr. Energy*, 2007, 32, 3842.

[33]. a) Z. Su and W. Zhou, *Adv. Mater*., 2008, 20, 3663. b) Z. Su and W. Zhou, *J. Mater. Chem.*,

2009, 19, 2301. c) Z. Su, G. Hahner and W. Zhou, *J. Mater. Chem*., 2008, 18, 5787.

[34]. X. Xu, X. Fang, T. Zhai, H. Zeng, B. Liu, X. Hu, Y. Bando, D. Golberg, *Small*, 2011, 7, 445.

Figure captions

Figure 1. (a-c) FESEM images of the as-anodized TiO_2 nanotubes with double-walled morphologies: (a) top-view , (b) bottom-view image, (c) cross-sectional image. The nanotubes are prepared under UV light with a power density of was 38 mW/cm^2. Scale bars of the inset images are 100 nm. (d) FESEM image of the as-anodized TiO_2 nanotubes prepared under UV illumination with a reduced power density of 20 mW/cm^2. (e) FESEM image of single-walled TiO_2 nanotubes prepared without UV illumination. (f) Schematic diagram showing the controlled formation of single- or double-walled TiO_2 nanotubes.

Figure 2. FESEM images (a – c) of the as-anodized TiO_2 nanotubes showing the formation of both double and single-walled nanotubes under UV-illumination in EG electrolyte containing 0.5% NH_4F and 0.2% H_2O at 60V, (d) schematic diagram showing the formation of double- walled TiO_2 nanotubes when UV was turned-on.

Figure 3. FESEM images of the top surface (a), TEM image (b) of the annealed double- walled TiO_2 nanotubes showing the nanopores and cracks formation in the walls of nanotubes after thermal annealing.

Figure 4. XRD patterns (a) and Raman spectra (b) of amorphous (blue curve) and anatase (red curve) double-walled TiO_2 nanotubes prepared in EG electrolyte containing 0.5% NH_4F and 0.2% H_2O under UV-illumination.

Figure 5. Photo-degradation behavior of methylene blue (MB) by annealed single and double-walled TiO_2 nanotubes and without TiO_2 nanotubes.

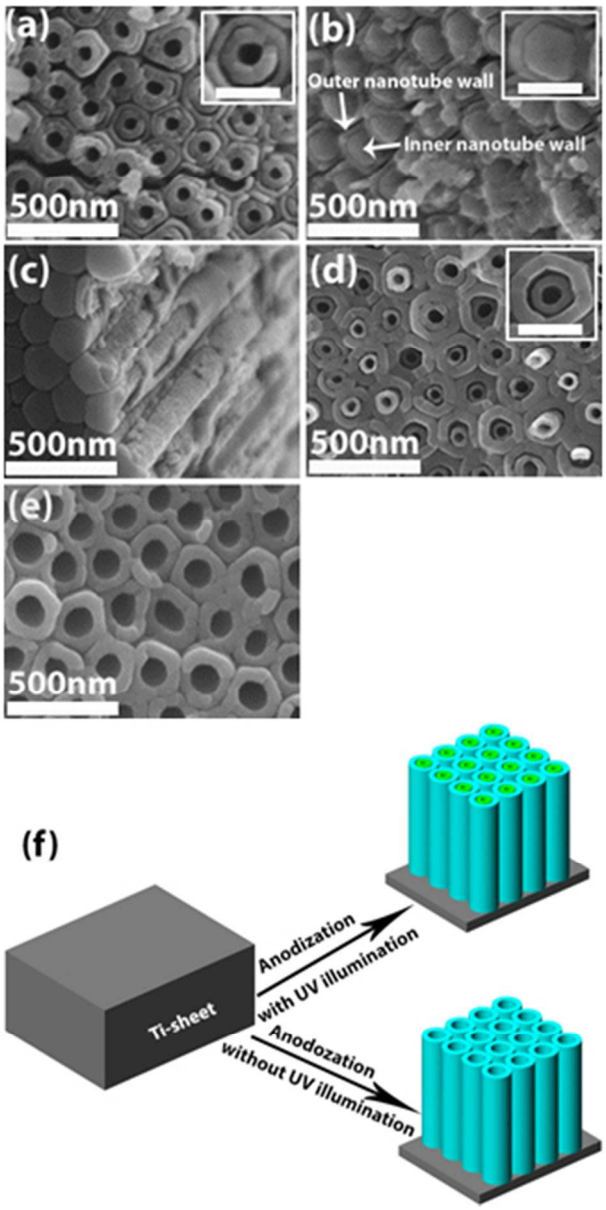

115x228mm (72 x 72 DPI)

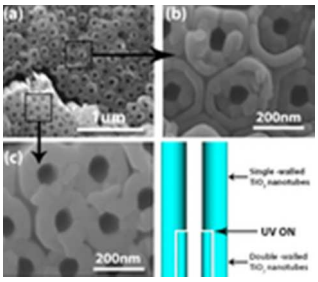

6x5mm (600 x 600 DPI)

4x1mm (600 x 600 DPI)

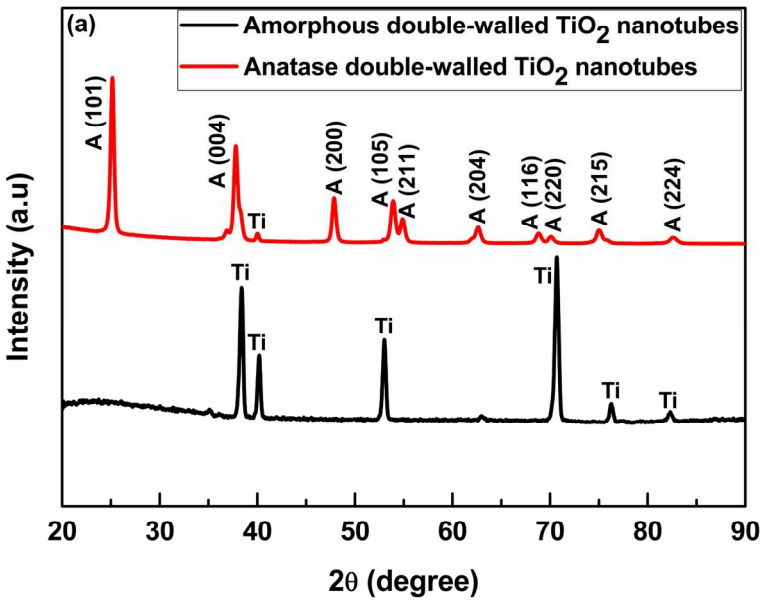

160x111mm (300 x 300 DPI)

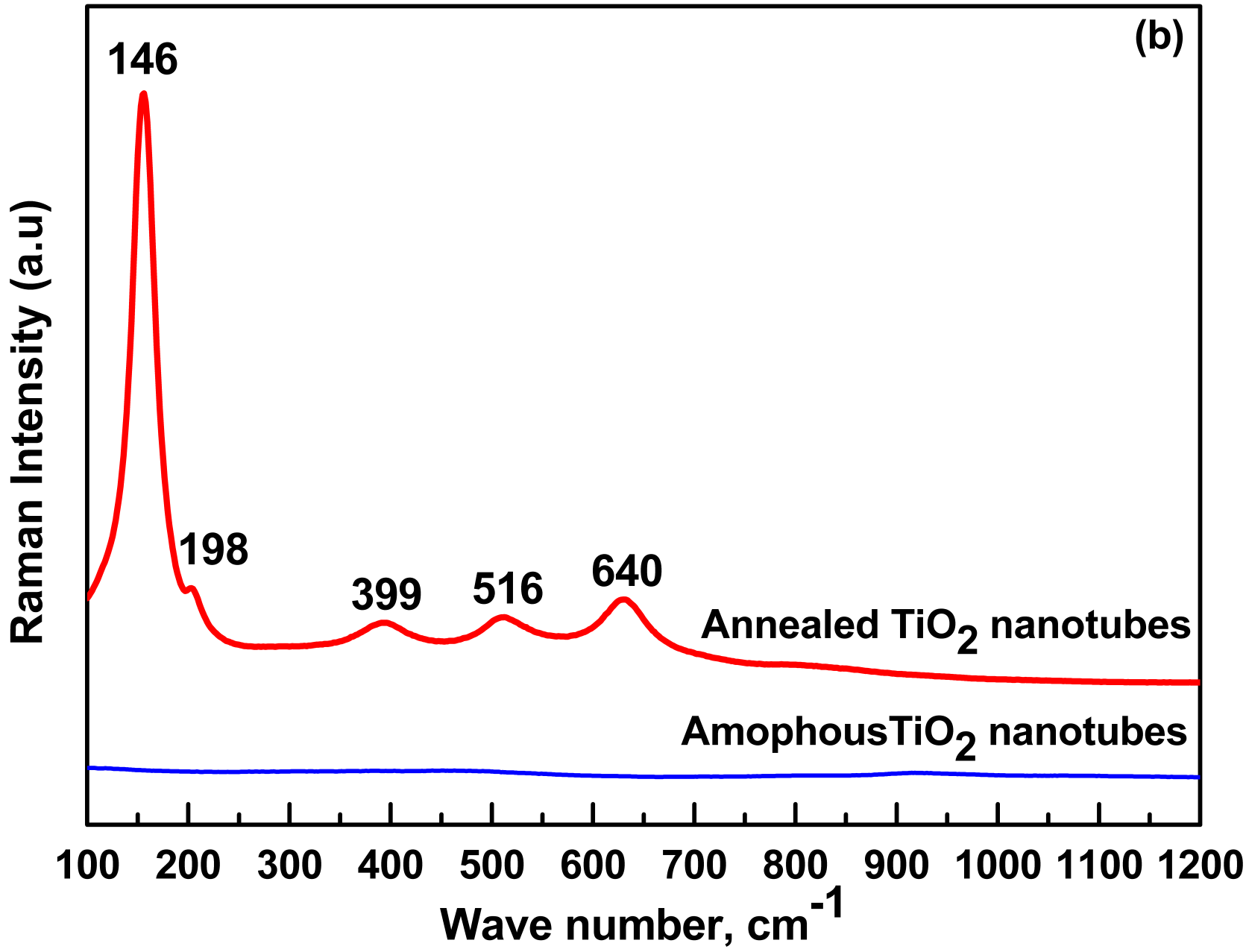

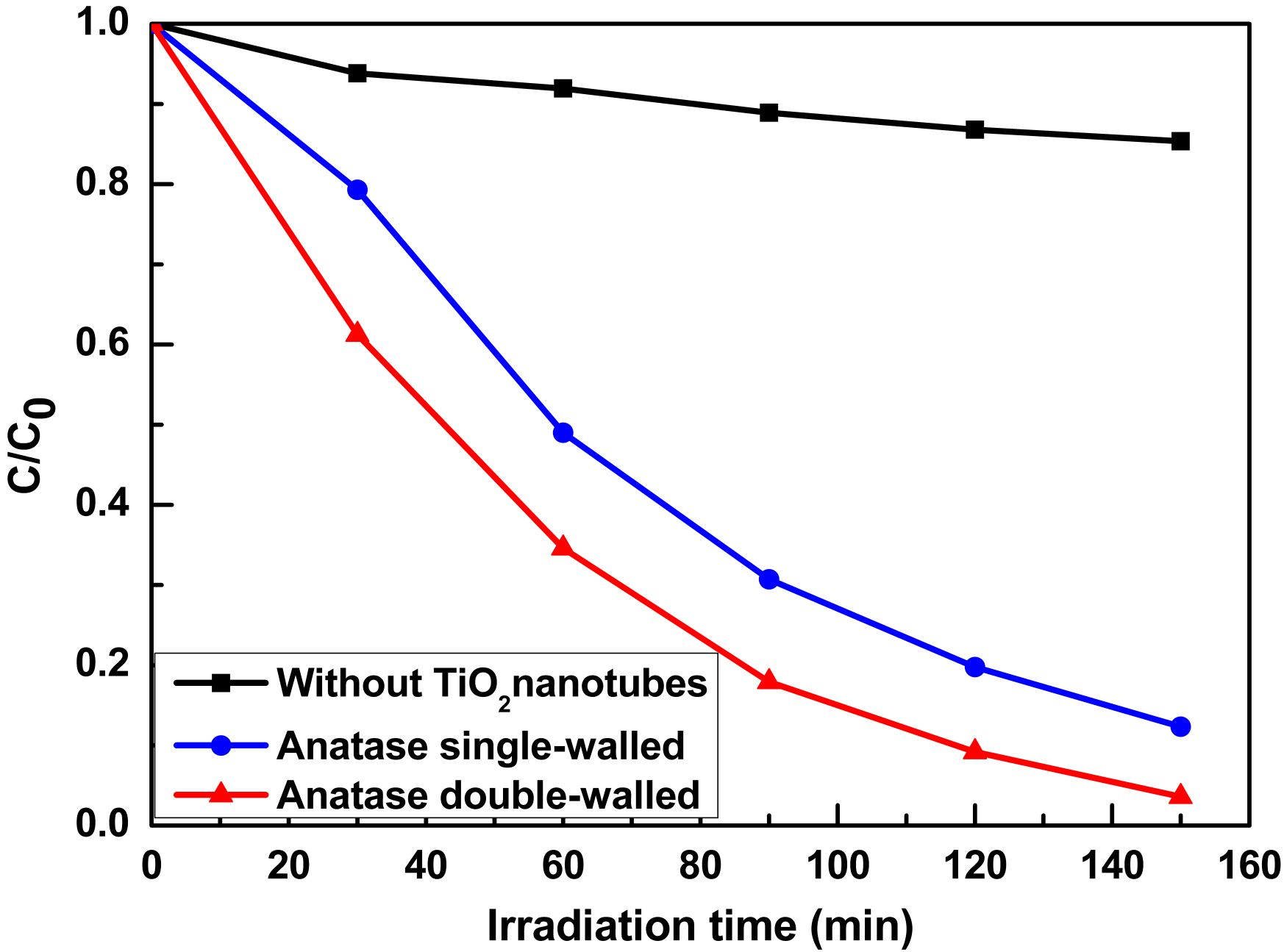

The table of contents entry

Double-walled TiO_2 nanotubes with porous wall morphologies are controllably fabricated by UV-assisted anodization. Double-walled or single-walled nanotubes can be selectively prepared by switching on/off UV light.